Electronic Supporting Information

Tetrazole functionalized benzoquinoline-linked covalent organic frameworks with efficient performance for electrocatalytic H_2O_2 production and Li-S batteries

Zhuangzhuang Wu,‡[a] Junming Luo,‡[a] Ying Liang,[a] Xinxin Yu,[a] Yuzhen Zhao,[a] Yongpeng Li,[b] Wenxin Wang,[a] Zhuyin Sui,*[b] Xinlong Tian*[a] and Qi Chen*[a]

[a] *State Key Laboratory of Marine Resource Utilization in South China Sea, Hainan Provincial Key Lab of Fine Chemistry, School of Chemical Engineering and Technology, Hainan University, Haikou, 570228, P.R. China. E-mail: tianxl@hainanu.edu.cn, chenqi@hainanu.edu.cn*

[b] *School of Chemistry & Chemical Engineering, Yantai University, Yantai 264005, P.R. China. E-mail: suizy@ytu.edu.cn*

* Corresponding Authors.

‡ These authors contributed equally to this work.

Characterization

Powder X-ray diffraction (PXRD) analysis was carried on a Bruker AXS D8 Advance Labx diffractometer using Cu Kα as X-ray source (λ = 1.5406 Å, 2 θ range 2-40°); Solid-state ^{13}C cross-polarization magic angle spinning nuclear magnetic resonance spectrum (^{13}C CP/MAS NMR) was recorded on a Bruker AVANCE III 500 MHz nuclear magnetic resonance spectrometer; X-ray photoelectron spectroscopy (XPS) was obtained by a Thermo Scientific ESCALAB 250Xi spectrometer with Al Kα radiation as the X-ray excitation source; High-resolution transmission electron microscopy (HRTEM), high-angle annular dark field scanning transmission electron microscopy (HAADF-STEM), and energy-dispersive X-ray (EDX) mapping of COF-TZ and Co@COF-TZ were performed on a Thermo Scientific Talos F200i S/TEM at an acceleration voltage of 200 kV; Nitrogen adsorption-desorption isotherms of various COFs-based materials were acquired by a Micromeritics ASAP 2460 automated sorption analyzer at liquid nitrogen (77 K).

Electrocatalytic oxygen reduction measurement

The ORR activity of COF-TZ in 0.1 M KOH was assessed with electrochemical measurements conducted on an electrochemical workstation (Ivium, The Netherlands) at room temperature (24 ± 2°C), using a three-electrode cell with a rotating ring-disk electrode (RRDE) system. The three-electrode cell made up a glassy-carbon-based working electrode, a graphite rod counter electrode, and an Hg/HgO reference electrode. All potentials in the thesis were quoted with reference to the reversible hydrogen electrode (RHE).

In order to explore the production rate of the H_2O_2 and ORR electron transfer mechanism, the electron transfer number (n) and H_2O_2 yield were calculated through the following equation:

$$n = \frac{4\,I_D}{I_D + I_R/N} \quad (1)$$

$$H_2O_2\% = \frac{200\,I_R/N}{I_D + I_R/N} \quad (2)$$

where I_R represent the absolute values of the ring current, I_D represent the absolute values of the disk current, and N = 0.37 represent the current collection efficiency at the Pt ring electrode.

Finally, the accelerated durability test (ADT) was carried out the COF-TZ in O_2-saturated 0.1 M KOH via chronoamperometric method for 36, 000 s at 0.6 V vs. RHE.

Li-S battery test

The CR2032 coin cells were assembled with Li-anode, S-cathode, separator, and electrolyte in an inert gas-filled glovebox. Among them, different S-cathodes were manufactured though mixing functional material (S@COF-CN, S@COF-TZ, or S-Co@COF-TZ composite), polyvinylidene fluoride, and carbon black (8:1:1, by weight) in N-methylpirrodinone, and sulfur loading was approximately 1.5 mg cm^{-2}; The Celgard 2400 membrane was served as a separator; The electrolyte was obtained via adding 1.0 wt% $LiNO_3$ into 1.0 M bis(trifluoromethane) sulfonimide lithium salt solution (1,2-dimethoxy ethane : 1,3-dioxolane = 1 : 1, by volume). The electrolyte/sulfur ratio is around 25 μL/mg per cell. The cyclic voltammogram and electrochemical impedance spectroscopy of different S-cathodes were recorded by

electrochemical workstation (CHI760E, Shanghai Chenhua). Discharge-charge performance of different functional materials were tested at the 2001 A.L Land battery.

Synthesis of TPB-DMTP-COF via Schiff base reaction

A mixed solvent of *o*-DCB (1 mL) and *n*-butanol (1 mL) was added to a Pyrex tube containing TAPB (56 mg, 0.16 mmol) and DMTA (46 mg, 0.24 mmol). The mixture was sonicated to complete dissolution and then HAc (0.2 mL, 6 M) was added. The air in the Pyrex tube was removed by freeze-pump-thaw cycles, then it was sealed through heating and heated at 120°C for 3 d. After the reaction stopped, the mixture was cooled, separated, and washed. At last, the solid powder was further purified by Soxhlet extractor filled with THF and dried at 60°C to obtain the TPB-DMTP-COF.

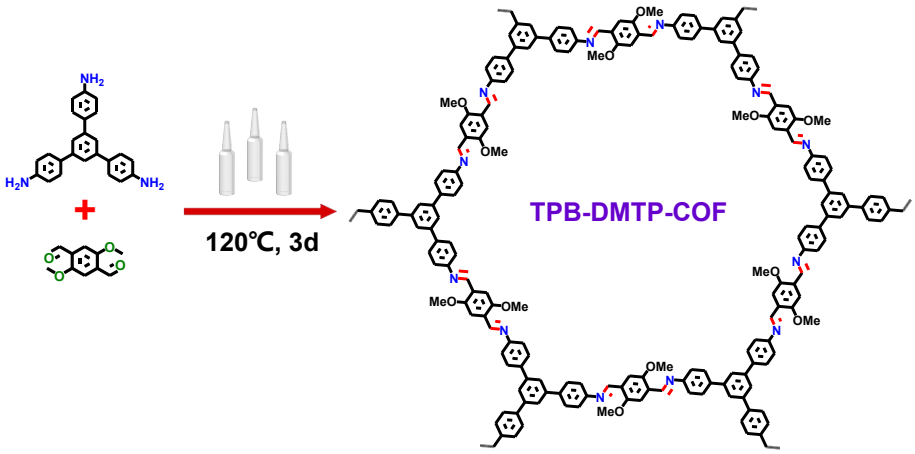

Scheme S1. Schematic representation of synthetic strategy for TPB-DMTP-COF.

Preparation of COF-CN by Povarov cycloaddition reaction

Typically, TPB-DMTP-COF (40 mg, 0.2 mmol), 4-cyanophenylacetylene (63.5 mg, 0.5 mmol), 2,3,5,6-tetrachloro-1,4-benzoquinone (74 mg, 0.3 mmol), toluene (6 mL), and $BF_3 \cdot OEt_2$ (20 μL) were sequentially added to a 25 mL round-bottom flask and then the mixture was stirred at 110°C for 72 h under argon atmosphere. Subsequently, the

precipitate was obtained via filtered, washed three times alternately with THF and saturated $NaHCO_3$ solution, respectively and dried at 60°C to get the COF-CN.

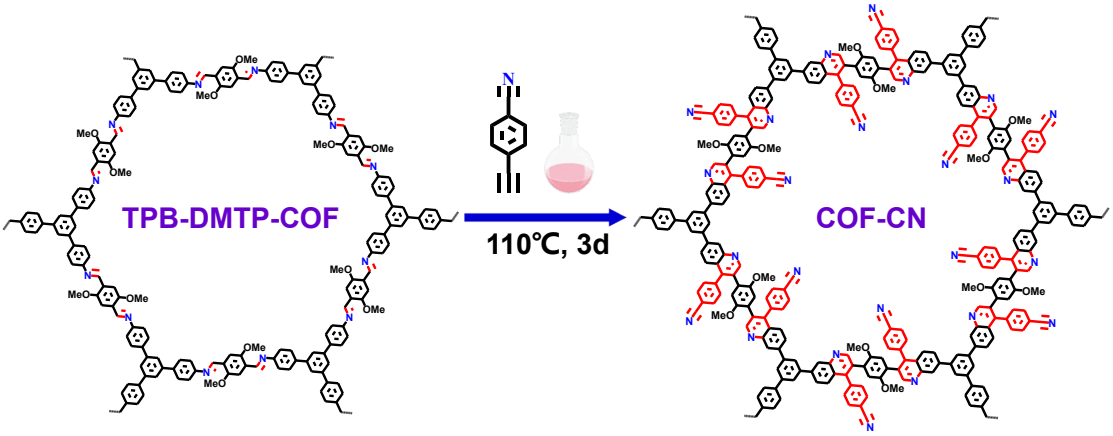

Scheme S2. Schematic illustration of the preparation process of the COF-CN.

Fabrication of S @COF-CN though sulfur melting and diffusing technique

S@COF-CN was obtained through a sulfur melting and diffusing technique. In brief, COF-CN and sublimed sulfur (mass ratio 3:2) were adequately mixed in a Teflon container and then heated at 155°C for 12 h to get S@COF-CN

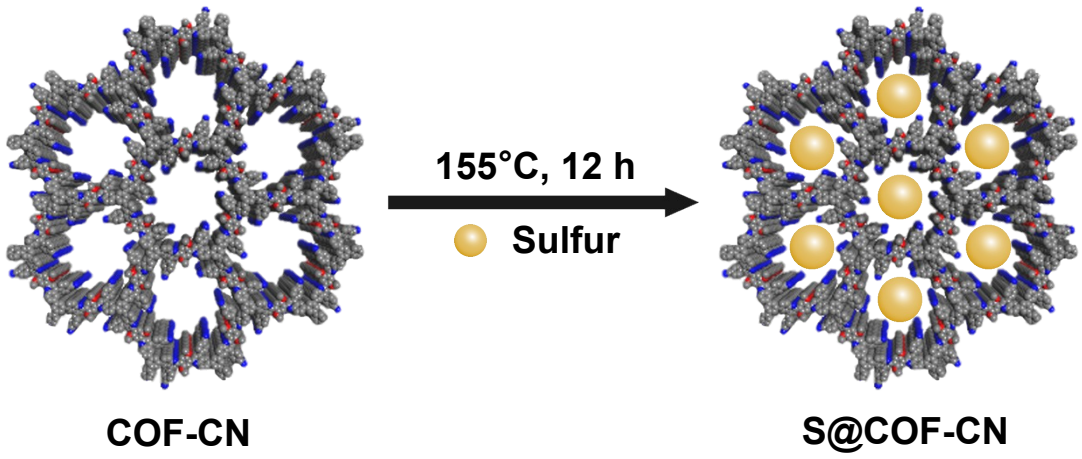

Scheme S3. Schematic representation of the transformation of COF-CN into S@COF-CN.

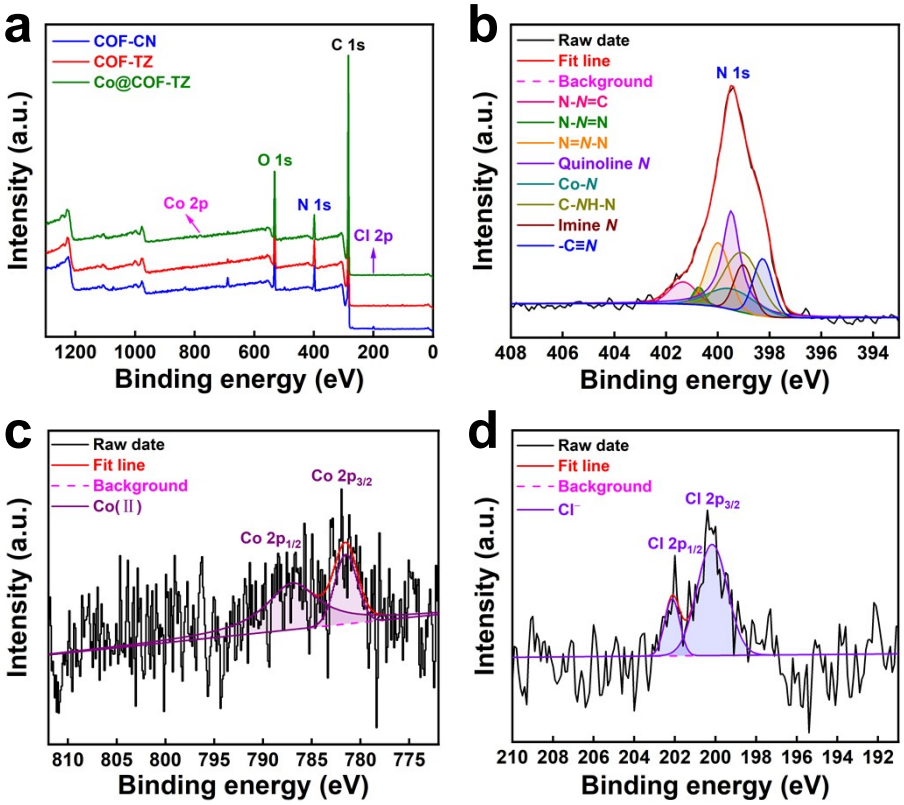

Fig. S1. (a) XPS survey scan of COF-CN, COF-TZ, and Co@COF-TZ; (b) N 1s XPS, Co 2p XPS, and (d) Cl 2p XPS of the Co@COF-TZ.

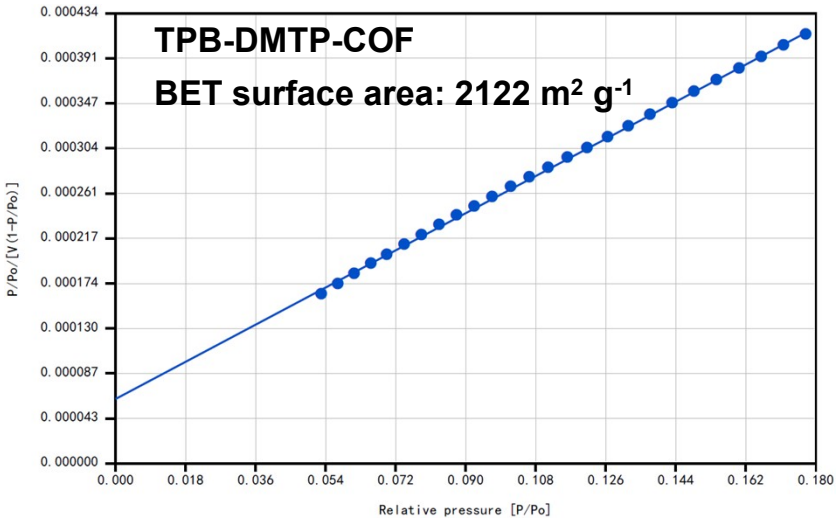

Fig. S2. BET surface area plot of TPB-DMTP-COF.

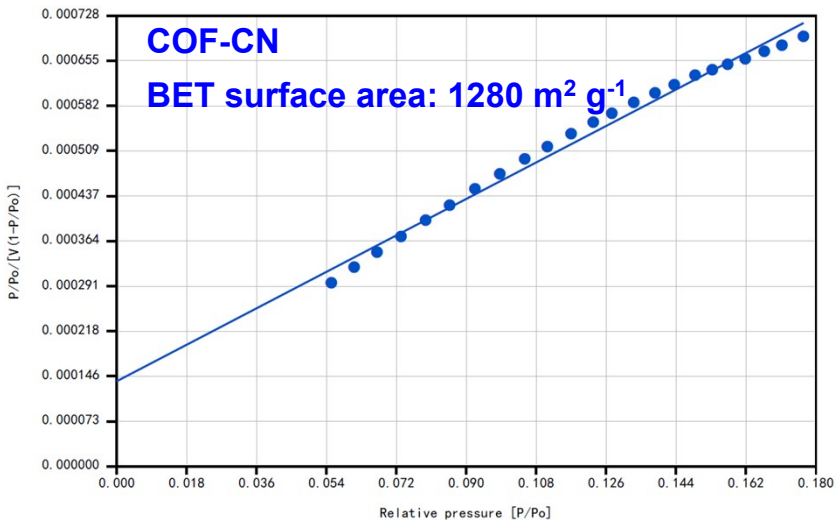

Fig. S3. BET surface area plot of COF-CN.

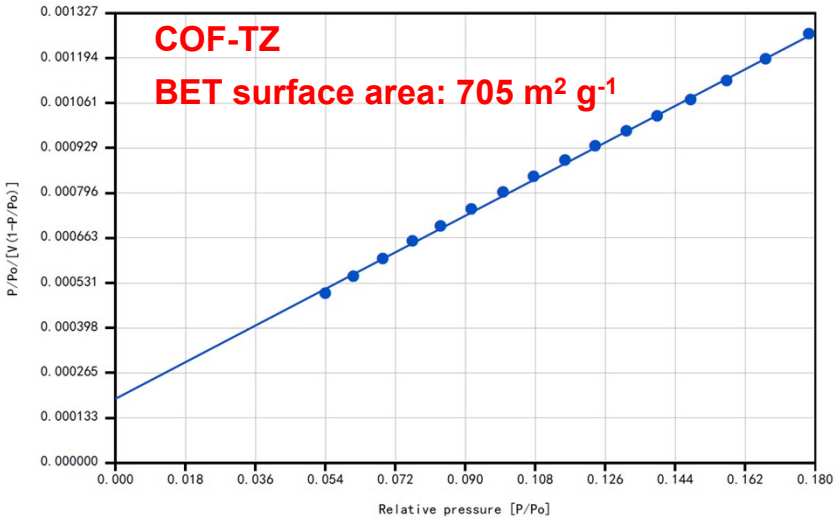

Fig. S4. BET surface area plot of COF-TZ.

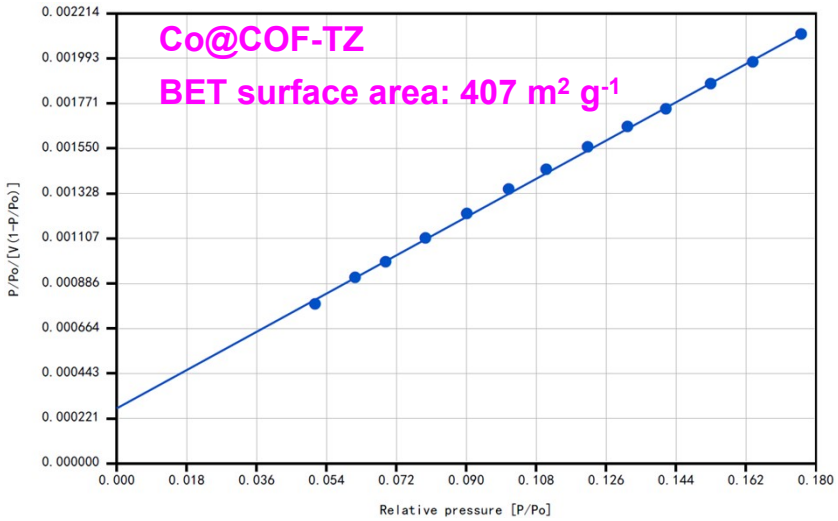

Fig. S5. BET surface area plot of Co@COF-TZ.

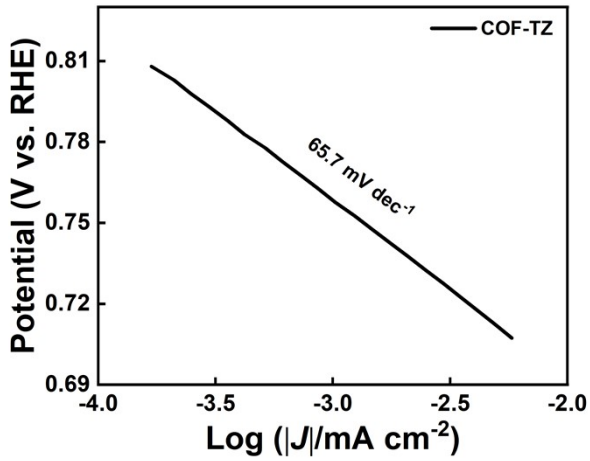

Fig. S6. Tafel plots of COF-TZ.

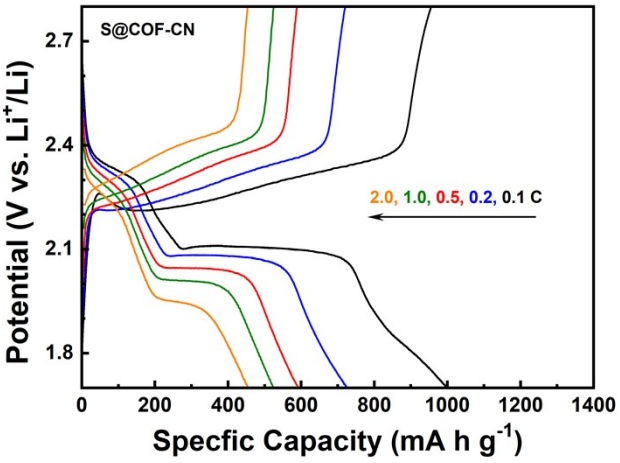

Fig. S7. Discharge-charge profiles of a S@COF-CN modified battery at different

rates.

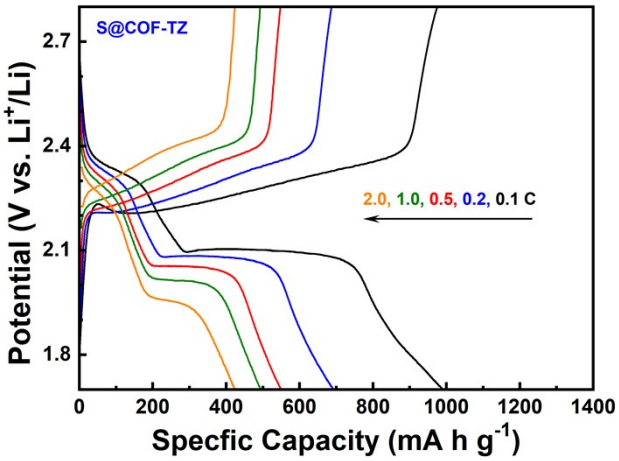

Fig. S8. Discharge-charge profiles of a S@COF-TZ modified battery at different rates.

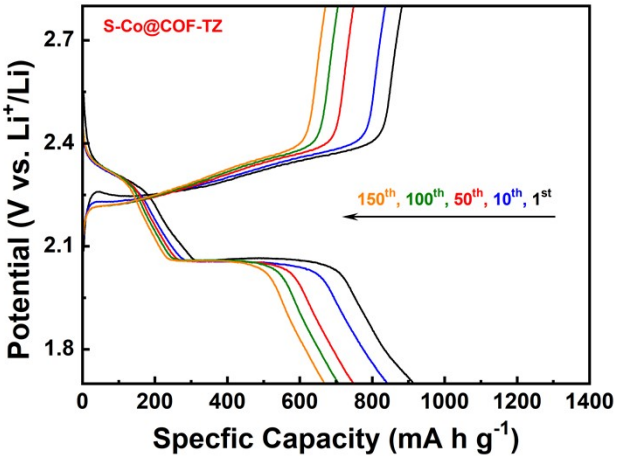

Fig. S9. Discharge-charge profiles of a S-Co@COF-TZ modified battery at 0.5 C for different cycles.

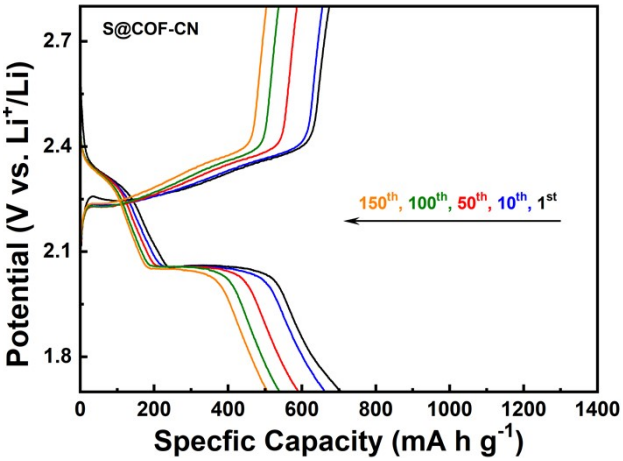

Fig. S10. Discharge-charge profiles of a S-@COF-CN modified battery at 0.5 C for different cycles.

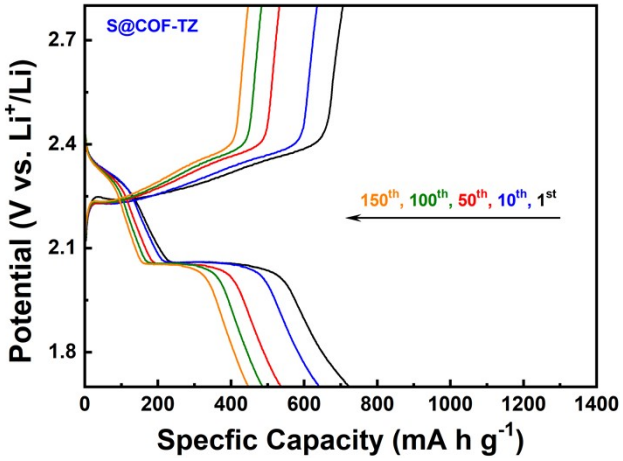

Fig. S11. Discharge-charge profiles of a S@COF-TZ modified battery at 0.5 C for different cycles.